Crack Tip Field of a Double-Network Gel: Visualization of Covalent Bond Scission through Mechanoradical Polymerization

Takahiro Matsuda[*,‡,#], *Runa Kawakami*[†,#], *Tasuku Nakajima*[‡,§,¶] and *Jian Ping Gong*[*,‡,§,¶]

‡Faculty of Advanced Life Science, Hokkaido University, N21W11, Kita-ku, Sapporo 001-0021, Japan. †Graduate School of Life Science, Hokkaido University, N21W11, Kita-ku, Sapporo 001-0021, Japan. §Soft Matter GI-CoRE, Hokkaido University. ¶Institute for Chemical Reaction Design and Discovery (WPI-ICReDD), Hokkaido University, N21W10, Kita-ku, Sapporo 001-0021, Japan. *e-mail: tkhr.matsuda@gmail.com, gong@sci.hokudai.ac.jp #These authors contributed equally.

Table of Contents (TOC) graphic (For Table of Contents Use Only)

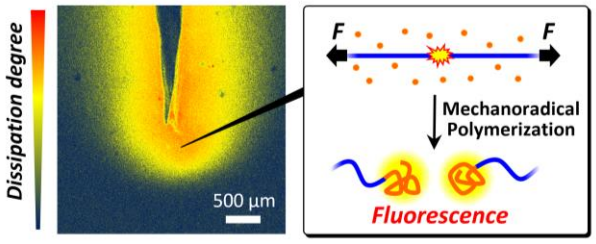

ABSTRACT

Quantitative characterization of the energy dissipation zone around a crack tip is the focal point in the fracture mechanics of soft materials. In this report, we present a mechanochemical technique for the visualization and quantification of the degree of polymer strand scission in the damage zone of tough double-network hydrogels. This technique uses mechanoradicals generated by covalent bond scission to initiate radical polymerization, which records the internal fracturing around the crack tip during crack opening or propagation. We adopted the mechanoradical polymerization of *N*-isopropylacrylamide, which forms a thermoresponsive polymer and whose distribution was visualized using an environment-responsive fluorescent probe. Two- and three-dimensional damage distributions were captured using a laser scanning confocal microscope. This technique also allowed for the quantitative estimation of the spatial distribution of stress, strain, and energy dissipation around the crack tip. The advantages and limitations of this technique are also discussed.

INTRODUCTION

Mechanically robust soft materials have garnered significant attention with respect to fundamental science[1–5] and the requirements of emerging applications, including medical implants,[6,7] soft robots[8,9] and wearable soft electronics.[10,11] For the practical application to ensure the mechanical reliability, toughness, i.e. crack resistance of the material, is crucially important as well as high strength and appropriate stiffness. Among the techniques of fabricating tough soft materials such as hydrogels and elastomers, the double-network (DN) concept[12] provides an effective and general strategy that is applicable to soft polymeric networks made using various chemistries.[13–18] Specifically, a DN material comprises two contrasting polymer networks: a brittle and sparse network and a stretchable and concentrated network,[13] customarily called the first and second networks, respectively, according to the sequence in the two-step synthesis. For a typical DN hydrogel, the concentrations of the first and second networks are 1–3 wt.% and 10–20 wt.%, respectively, and the rest is water. Even while possessing 80–90 wt.% water, a DN gel exhibits remarkably high fracture toughness of 100–5000 J m^{-2} that is one or two orders of magnitude higher than that of the conventional hydrogels.[13,19–21] It has also been reported to exhibit high resistance of fatigue fracture.[22]

Previous studies have shown that the extraordinarily high fracture toughness of the DN gels, or multiple-network elastomers that use the DN concept, is attributable to the scission of covalent bonds of the first network strands, referred to as *internal fracturing*.[13,17,23–27] The internal fracturing results in the formation of a large *damage zone*[28–31] around a crack tip where the stress is highly concentrated. A large amount of mechanical energy is dissipated to form the damage zone prior to the crack progress, analogous to a Dugdale plastic zone of metals and a local

crazing of glassy polymers, resulting in high fracture toughness. Therefore, quantitative characterization of the damage zone is the focal point in fracture mechanics of tough DN gels.

The damage zone of a DN gel has been characterized via optical microscope observation of the structural heterogeneity induced by internal fracturing.[31,32] Yu et al. observed the damage zone with a size of several hundred micrometers using a three-dimensional (3D) violet laser scanning microscope.[31] Liang et al. then distinguished three regions (hardened zone, yielded zone, and pre-yielding zone) in the damage zone of a thin (100 μm thick) DN gel using a phase-contrast optical microscope as well as the 3D violet laser scanning microscope.[32] While these optical observations can directly identify the damage zone, quantification of the degree of internal damage and its spatial distribution is difficult. Furthermore, re-swelling treatment of the sample is required after the fracture, which causes the overestimation of the size of the damage-zone. Hence, a new technique that enables the quantitative characterization of as-fractured DN gels is required.

Recently, mechanochemical techniques (i.e., chemical transformation induced by mechanical force) have been proposed to investigate the mechanics of polymeric materials.[17,33–42] In typical mechanochemical sensing, force-responsive molecules (called mechanophores) are chemically incorporated into the polymer backbone or crosslinking point. For example, internal fracturing around the crack tip of a multiple-network elastomer was visualized using a dioxetane mechanophore that emitted light when it broke.[17] Chain scission at the fractured surface of a hydrogel was visualized by scission-induced fluorescence of π-extended anthracene adducts.[40] This mechanochemical technique can also provide quantitative information on bond scission,[17,37,40] and is potentially applicable to DN gels.[43] However, the requirement of

mechanophore incorporation often limits its extensive application. Furthermore, direct mechanophore incorporation may affect the network structure or mechanical properties of the materials.[17,37]

In this study, we propose a novel mechanochemical technique for the visualization and quantification of the bond scission of DN gels without using a designed mechanophore, inspired by our recent finding.[27] The technique is based on the combination of mechanoradical polymerization and fluorescence microscopy, as conceptually illustrated in **Figure 1**. Specifically, the internal fracture of a DN gel generates a large amount of mechanoradicals at the ends of the broken first network strands.[27] These mechanoradicals are used to initiate the polymerization of the pre-loaded monomer *N*-isopropylacrylamide (NIPAAm), thus forming a temperature-responsive polymer poly(*N*-isopropylacrylamide) (PNIPAAm).[44] The PNIPAAm chains tethered at the broken ends of the first network are visualized using a pre-loaded fluorescent molecule, 8-anilino-1-naphthalenesulfonic acid (ANS), that exhibits strong fluorescence in the hydrophobic environment.[45,46] Since PNIPAAm becomes hydrophobic above its lowest critical solution temperature (LCST) at approximately 30–35 °C,[44] ANS exhibits strong fluorescence in the damaged region above the LCST. Therefore, by using a laser scanning confocal microscope (LSCM), two-dimensional (2D) or 3D images of the damage zone can be captured without the re-swelling treatment of the samples. In this study, we first visualize the damage zone of a DN gel using this method. Then, we demonstrate the extraction of the spatial distributions of stress, strain, and dissipated energy density from the quantitative fluorescence result. We also discuss the advantages and limitations of this technique in comparison with other methods.

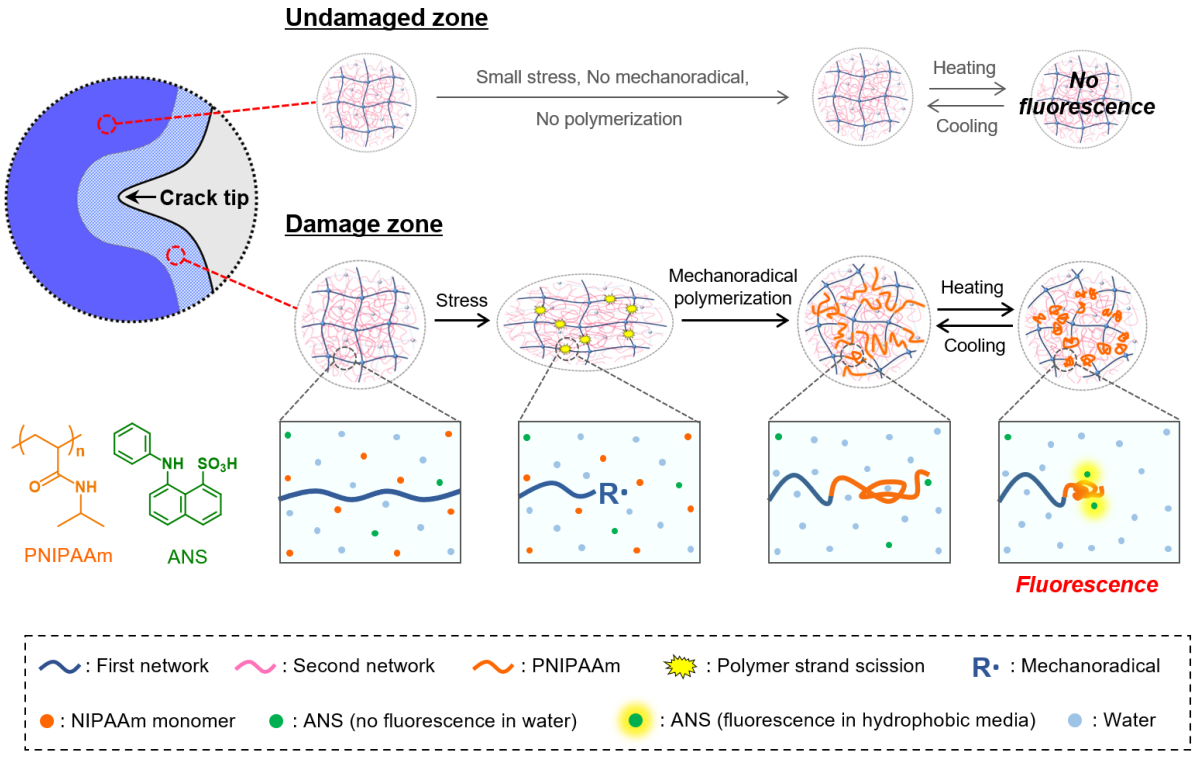

Figure 1. Conceptual scheme representing a visualization of the damage zone where internal fracturing of the first network occurred around the crack tip in the DN gels. In the damage zone, the mechanoradicals generated by polymer strand scission initiate the polymerization of NIPAAm to form PNIPAAm, a thermo-responsive polymer showing LCST-type micro-phase separation. Because the fluorescent molecule ANS exhibits strong fluorescence only in the hydrophobic environment, the damaged region is visualized when observed at a temperature that exceeds the LCST of the PNIPAAm while the undamaged region hardly exhibits fluorescence. The fluorescence image and spatial distribution of fluorescence intensity around the crack tip or a fractured surface are obtained using a laser scanning confocal microscope (LSCM).

EXPERIMENTAL SECTION

Materials. DN gels comprising a poly(2-acrylamido-2-methylpropane sulfonic acid sodium salt) (PNaAMPS) first network and a polyacrylamide (PAAm) second network were synthesized (see Supporting Information).[19,27] The synthesized DN gels were immersed in a large volume of deionized water for at least one day before the following experiments were conducted.

Mechanoradical polymerization via tearing. To induce mechanoradical polymerization at the damage zone through tearing fracture, a DN gel containing NIPAAm and ANS was torn in an argon glove box.[27] First, a DN gel was cut into a trouser shape (thickness ~3 mm, full width 8 mm, each leg's width 4 mm, full length ~50 mm, and initial cut length ~20 mm). The trouser-shaped gel was immersed in a filtered aqueous solution of 1.0 M NIPAAm and 200 mg L^{-1} ANS (in typical) for 1 day in an argon glove box at ~15 °C to supply NIPAAm and ANS into the gel and to remove the oxygen from the gel. Afterwards, the sample containing NIPAAm and ANS was torn using a tensile tester (MCT-2150, A&D Co.) at a crosshead velocity of 100 mm min^{-1} in the glove box at ~15 °C. After tearing, the gel was wrapped with plastic film (Saran wrap) to avoid drying, and stored in the glove box overnight (~18 h) to allow for mechanoradical polymerization.

Mechanoradical polymerization via stretching. A procedure that was similar to the one above was used for the mechanoradical polymerization of NIPAAm induced by stretching. A dumbbell-shaped DN gel (standardized to JIS-K 6251-7; 12-mm gauge length, 2-mm width, and ~3-mm thickness) was immersed in a filtered aqueous solution of 1.0 M NIPAAm and 200 mg L^{-1} ANS for 1 day in an argon glove box (~15 °C). The sample was then stretched using a tensile tester to a certain displacement, and then unloaded to the original length. The crosshead velocity

was 100 mm min^{-1}. The imposed maximum strain, ε_{max}, was calculated from the distance between two dots applied on the gel measured using a caliper. The stretched gel was wrapped with plastic film and stored overnight in the glove box. For this test, individual test pieces were used for each strain imposed (ε_{max} = 0.5, 0.6, 0.8, 1.5, 2.1, or 3.3).

Fluorescence spectroscopy. Fluorescence spectra were obtained at 45 ℃ using a fluorometer (FP-6600, Jasco Co.) equipped with an epifluorescence unit (EFA-383, Jasco Co.). The excitation wavelength was 402 nm.

Fluorescence observation using a laser scanning confocal microscope (LSCM). Fluorescence microscopic measurements were carried out using a laser scanning confocal microscope (LSCM) (Nikon A1 Rsi and Ti-E, Nikon Co.) equipped with a Plan Fluor x4 objective lens (NA 0.13, Nikon Co.). The excitation laser wavelength was 402.5 nm. Fluorescence emission was measured within a wavelength range of 425–475 nm. For all measurements, the sample was placed in a glass-bottom dish (3970-035-SK, IWAKI & Co.) and maintained at 42 °C (above the LCST of PNIPAAm) using a stage-top incubator (INUBG2H-TIZB, Tokai Hit Co.). For qualitative observation (**Figures 3, 5, 6, and S2**), the excitation laser intensity was tuned to appropriate values to obtain clear images. For quantification purposes (**Figures 7, 8, and S4**), the same laser intensity was used for all measurements. The background intensity was subtracted from the intensity data in the quantitative results.

Tensile test for mechanical characterization. Uniaxial and uniaxial cyclic tensile tests were carried out in air at a crosshead velocity of 100 mm min^{-1}.[25] The detailed procedure is presented in the Supporting Information.

RESULTS and DISCUSSION

Mechanoradical polymerization and fluorescence emission

First, we investigated the mechanoradical polymerization of NIPAAm in a stretched DN gel and the resulting fluorescence behavior of the sample. All fluorescence measurements were carried out at relaxed (stress-released) states of the gels. Hereafter, the "unstretched" gel denotes a sample to which no stretch was applied (strain $\varepsilon_{max} = 0$), and "stretched" gel denotes a sample to which a prescribed stretch ($\varepsilon_{max} > 0$) was applied. After the stretch was released, the length of the stretched gel almost returned to the original length in the relaxed state. **Figure 2a** shows the optical images of the unstretched ($\varepsilon_{max} = 0$) and stretched ($\varepsilon_{max} \approx 4$) DN gels fed with NIPAAm and ANS observed at 45 °C. The unstretched DN gel was transparent, while the stretched one was opaque. The opaque appearance of the stretched sample indicates that NIPAAm in the DN gel was polymerized by the mechanoradicals, and the synthesized PNIPAAm underwent micro-phase separation above the LCST. The monomer conversion was determined to be approximately 40% in this typical case (see **Figure S1**). We also confirmed the presence of strong fluorescence using a fluorescence spectrometer with an excitation wavelength of 402 nm. As shown in **Figure 2b**, the stretched gel exhibits strong fluorescence at approximately 470 nm, while the unstretched gel shows negligible fluorescence. This result demonstrates that internal fracturing in a deformed DN gel can be detected by fluorescence.

Next, we observed the damage zone around the fractured surface of the DN gel. **Figure 2c** shows the optical images of a trouser-shaped DN gel torn by hand. As expected, only the region around the torn surface becomes opaque under visible light (**Figure 2c(i)**) and exhibits strong fluorescence under UV light (**Figure 2c(ii)**). These results clearly indicate that internal

fracturing occurred around the crack tip during the tearing of the sample. The damage zone from the fractured surface to the bulk is several millimeters thick, which is close to the value observed in previous reports on DN gels (0.1–0.9 mm)[31,32] and multiple-network elastomers (several millimeters).[17]

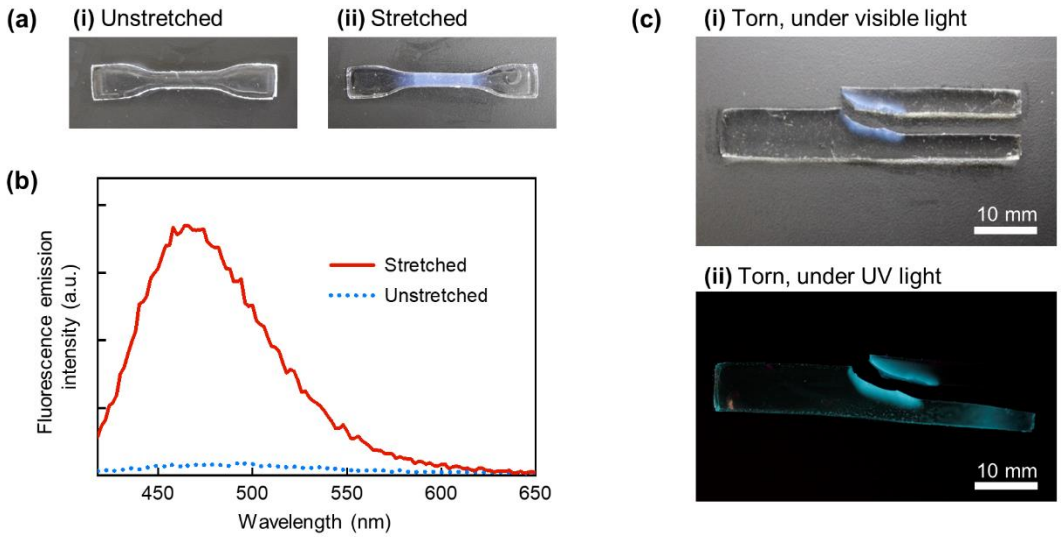

Figure 2. (a) Optical images of **(i)** unstretched and **(ii)** stretched ($\varepsilon_{max} \approx 4$) DN gels fed with NIPAAm and ANS under visible light observed at 45 °C. **(b)** Fluorescence spectra (excitation: 402 nm) of the corresponding DN gels at 45 °C. **(c)** Optical images of a torn DN gel fed with NIPAAm and ANS observed at 45 °C under **(i)** visible light and **(ii)** UV light (365 nm).

Fluorescence imaging using LSCM

Using a laser scanning confocal microscope (LSCM), we visualized the two- and three-dimensional fluorescence images of a torn sample. **Figure 3a** shows an optical image of the trouser-shaped specimen torn for several millimeters. A strongly opaque region around the crack tip, which is consistent with **Figure 2c(i)**, is observed. **Figure 3b** shows a two-dimensional fluorescence image obtained from a depth of 5 μm of the sample surface. A fluorescent region with an arc shape in front of the crack tip and strip-shape along the fractured surface, corresponding to the damage zone, is observed. **Figure 3c** shows a three-dimensional image around the crack tip from the top surface to the bottom surface of the gel. The image is constructed from two-dimensional images measured at different depths from the top surface.

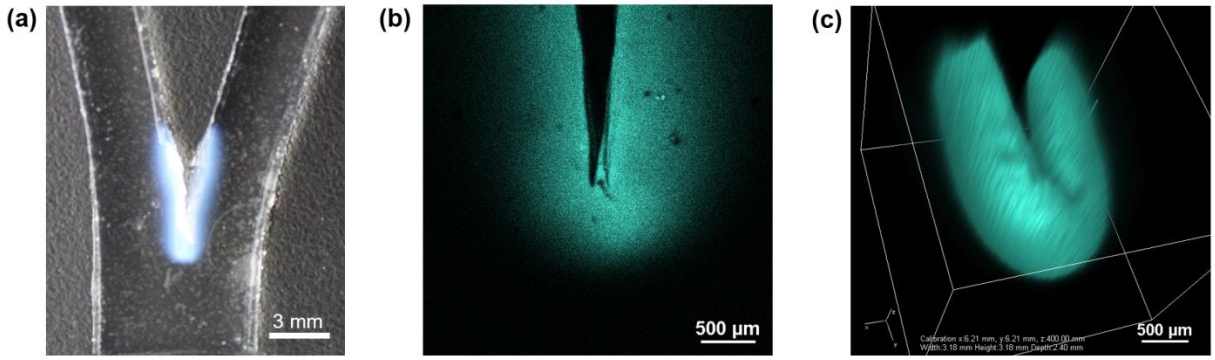

Figure 3. (a) An optical image, and **(b)** two-dimensional and **(c)** three-dimensional fluorescence images obtained using a laser scanning confocal microscope (LSCM) around the crack tip of a torn DN gel fed with NIPAAm and ANS observed at 42 °C.

Fluorescence intensity profile

Next, we measured the fluorescence intensity profile in the damaged zone using a trouser-shaped specimen (**Figure 4**). To facilitate the discussion afterwards, we set the coordinate for a fractured piece in the relaxed state, as shown in **Figure 4** (right). The fractured surface was set in the xy plane with $z = 0$, the crack advanced direction was set along the x-axis, y was set as zero on one of the sample surfaces, and the z-axis was assigned positive values within the sample. The in-plane (xz plane) observation using LSCM was performed at a depth $y = 5$ μm from the gel surface (see **Figure 4**). The fluorescence intensity profile $I(z)$ was obtained by line scan, at a step of 6.2 μm, along the z-direction from the fractured surface ($z = 0$) to the bulk ($z \approx 2000$ μm). The raw data contained relatively strong noise (**Figure S2**), which may have originated from equipment such as from detector sensitivity and/or from the sample such as from the micro-scale inhomogeneity of the internal fracturing. Hence, in this study, we show moving-averaged data over 9 data points, which give an average over a length scale of ~50 μm in the z-direction (see **Figure S2** for details). This length taking average (~50 μm) is significantly smaller than the size of the damage zone of the DN gels being studied.

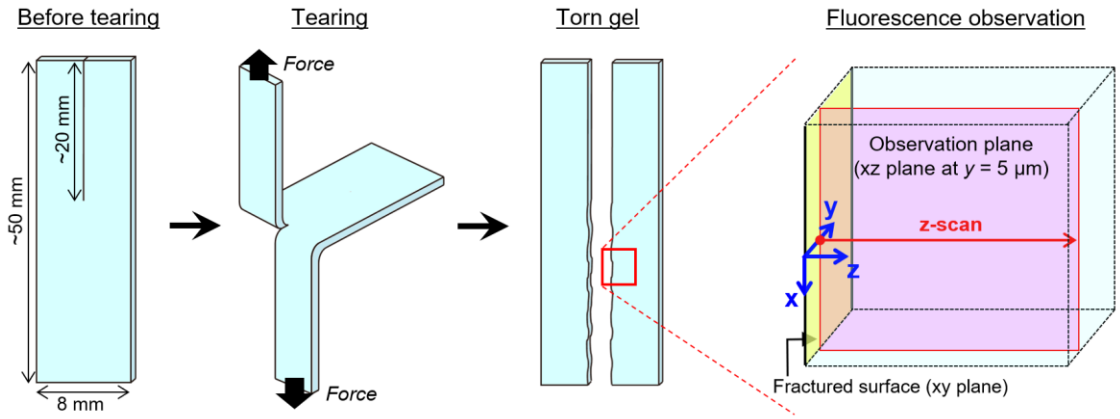

Figure 4. Schematic of the tearing test of a trouser-shaped DN gel and the observation plane of the fluorescence image obtained using LSCM. The fluorescence intensity images were obtained in the xz plane that is vertical to the fractured surface (xy plane), and the line scans were performed along the z-axis, 5 μm beneath the sample surface.

A typical LSCM image and the corresponding fluorescence intensity profile of a torn DN gel are shown in **Figures 5a(i) and 5b(i)**, respectively. The fluorescence intensity, which reflects the degree of polymer strand scission as discussed later, shows a gradient distribution in the damage zone. It maximizes near the fractured surface and decreases gradually from the surface to the bulk. The damage zone extends over approximately 2000 μm.

This technique clearly reveals that the damage zone profile strongly depends on the fracture method. When the DN gel was cut using scissors and a razor blade, the damage-zone thickness decreased to ~700 μm and ~500 μm, respectively (**Figures 5a(ii), 5a(iii), 5b(ii) and 5b(iii)**), while the maximum intensity near the fractured surface was almost the same as that of the torn sample. Because these observations were performed under the same experimental conditions, these results suggest that the applied stress and deformation near the cut surface hardly depend on the fracture method, while the stress and strain fields away from the crack tip are dominated by the fracture method. It is worth mentioning that, in some practices, internal damage within the range of ~100s μm is possibly presented even when a DN gel is cut using a razor blade.

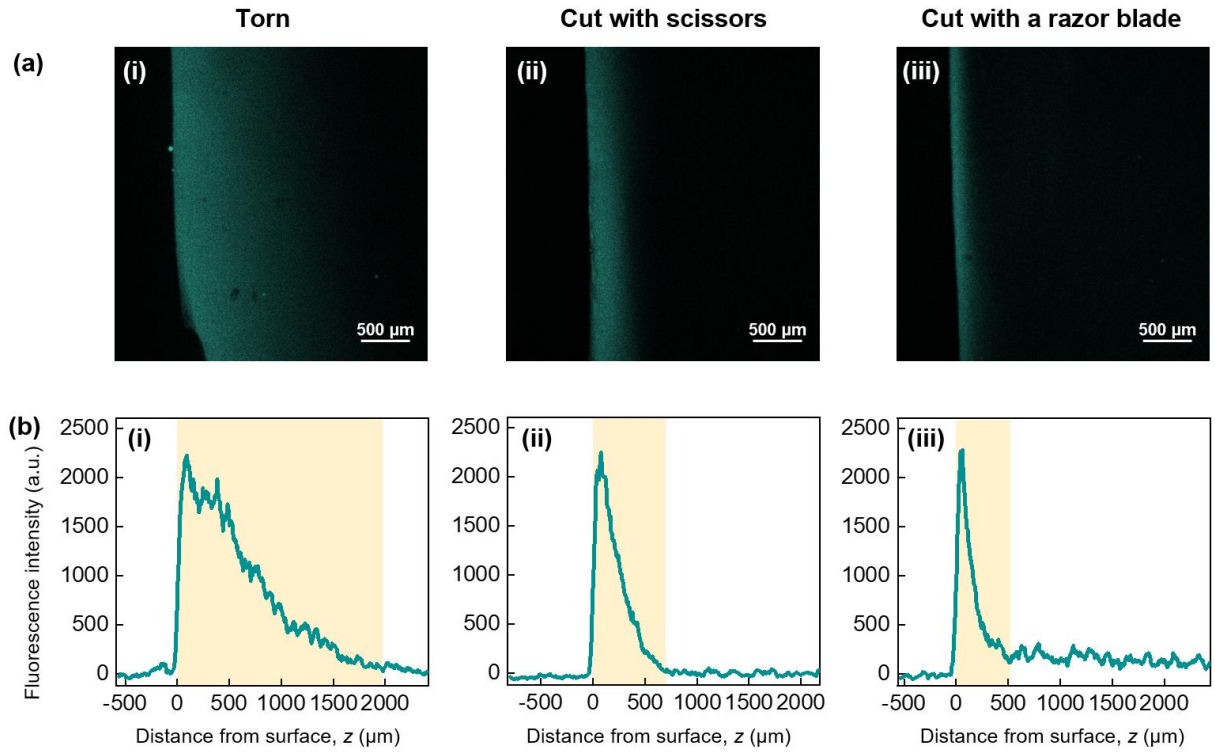

Figure 5. (a) Fluorescence images and **(b)** line profiles of fluorescence intensity $I(z)$ of the DN gels from fractured surface to bulk. The DN gel was ruptured using different methods including being, **(i)** fractured by tearing using a trouser-shaped sample (see **Figure 4**), **(ii)** cut using scissors, and **(iii)** cut using a microtome razor blade. Yellow highlighted regions in **(b)** roughly denote the damage zone. The same experimental condition was used for these three individual experiments. The profiles in **(b)** are the moving-averaged data (see **Figure S2**).

Spatial resolution

The spatial resolution of this method is limited by two factors: the size of PNIPAAm tethered to the partially broken first network and the resolution of LSCM. To estimate the maximum possible size of the tethered PNIPAAm chain, we assumed that the maximum polymerization degree, N, of PNIPAAm was 10^6 (molecular weight of ~10^8 g mol^{-1}). The radius of the PNIPAAm chain in a random coil state was roughly approximated as $aN^{1/2} \sim 250$ nm, where a was the length of the monomer unit ($a \approx 0.25$ nm). At 42 ℃, the PNIPAAm chain in the globule conformation above its LCST must be smaller. Therefore, the size of the PNIPAAm chain under observation should be smaller than ~100s nm. On the other hand, the resolution of LSCM, depending on the optical setup, is usually not smaller than 100 nm. For example, the theoretical optical resolution of LSCM used in this work was ~1 μm in the observation plane, considering the objective lens (numerical aperture 0.13) used under air (refractive index 1.0) and excitation wavelength (402 nm). Therefore, the theoretical resolution of this technique is usually not limited by the size of the PNIPAAm chain, but rather by the optical system. Note that our LSCM setup is at a relatively low-resolution condition in order to capture a wide field image. A sub-micrometer resolution is potentially achieved with an improved optical system. In the present study, however, the 9-points moving-average (~50 μm) was processed in the intensity profiles to reduce the noise, as mentioned above. Hence, the resolution of the proposed data is expected to be ~50 μm, which is still significantly smaller than the thickness of the damage-zone observed in the DN gels. We believe that the noise can be reduced by improving the optical system or the fluorescent probe.

To confirm the spatial resolution experimentally, we observed a fractured surface of a single-network hydrogel. For the fracture of a single-network gel, only the surface network layer is expected to break upon crack propagation[47,48] and the polymer scission inside the gel is negligible.[24,27] Therefore, the surface damaged region of a single-network gel is considered to be the network mesh scale (~10^0–10^2 nm), which is smaller than the resolution in our method. In this experiment, a PNaAMPS single-network gel fed with NIPAAm monomer and ANS fluorophore was broken by bending owing to the stiffness and brittleness of this gel. As shown in **Figures 6a and 6b**, the left leg of the PNaAMPS gel was broken in the argon atmosphere to allow for mechanoradical polymerization, while the right leg was broken in air as a control to inhibit mechanoradical polymerization by oxygen. Observation using LSCM showed a clear fluorescent line at the left fractured surface only (**Figure 6c**). This fluorescence is not a result of the surface effect (such as the drying effect) but rather mechanoradical polymerization because such fluorescence was not observed on the right side where mechanoradical polymerization was inhibited. The moving-averaged fluorescence profile (**Figure 6d**) indicates that the thickness of the fluorescence around the fractured surface is ~60 μm which is very close to the expected resolution of ~50 μm. This result also demonstrates that this technique is applicable not only to the fracture of DN gels but also to the fracture of other materials accompanied by homolytic bond scissions. Spatial resolution should be improved for some applications.

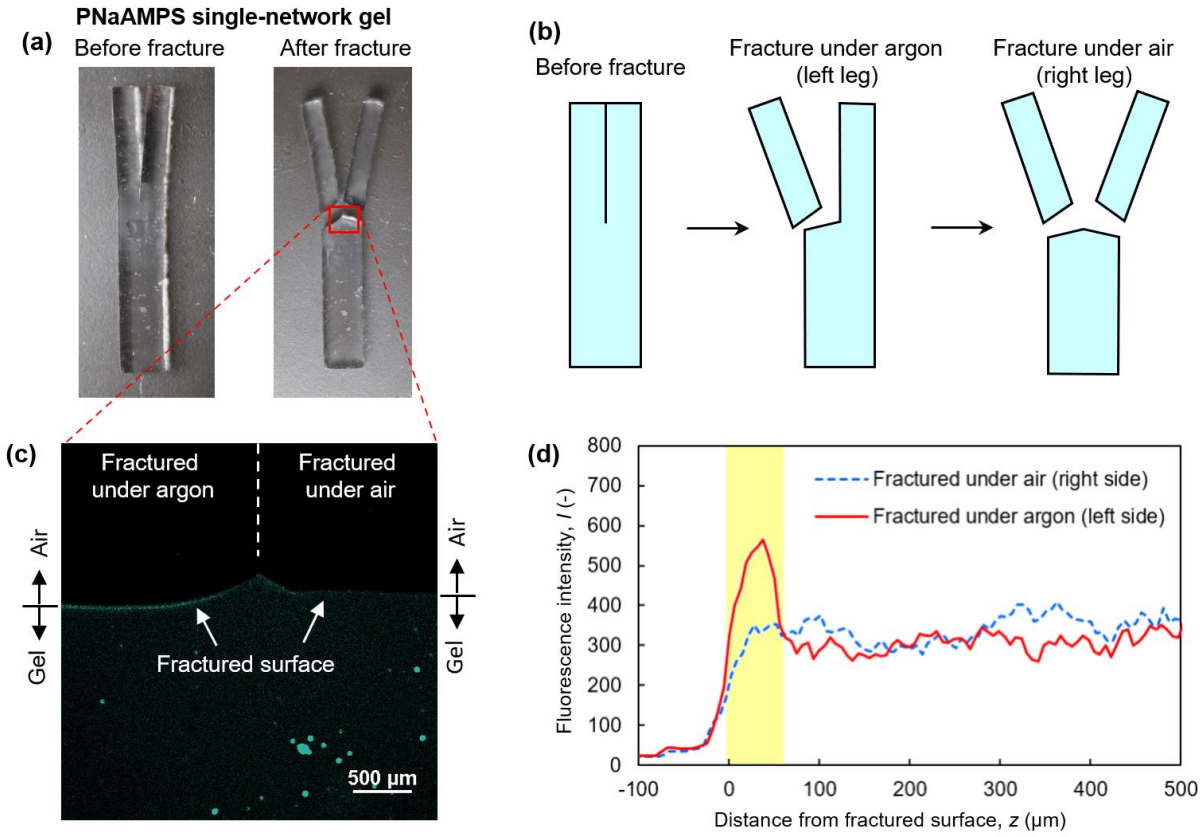

Figure 6. Mechanoradical polymerization around the fractured surface of a PNaAMPS single-network gel. **(a)** Optical images of the PNaAMPS gel before and after fracturing. **(b)** Schematic of the fracture method. **(c)** Fluorescence image obtained using LSCM. **(d)** Fluorescence intensity profiles of the fractured PNaAMPS gel. Fluorescence around the fractured surface was observed only on the left side (yellow highlight region in (d)) because the mechanoradical polymerization on the right side was inhibited by oxygen under air. The profiles are the moving-averaged data.

Quantitative characterization

In principle, the fluorescence intensity, I, reflects the damage degree because the intensity depends on the amount of PNIPAAm that correlates to the mechanoradical concentration. In previous studies, the damage degree of DN gels was typically characterized as the dissipated mechanical energy density, U_{diss} (unit of J m^{-3}), that is obtained from the mechanical hysteresis in cyclic tensile tests.[24,25,49] Recently, U_{diss} has also been found to correlate well with mechanoradical concentration.[27] In this section, we first clarify that I exhibits good correlation with U_{diss}; then we demonstrate the quantitative characterization of the damage zone.

We used a DN gel whose tensile stress–strain curve is shown in **Figure 7a**. This DN gel shows a typical tensile property that accompanies yielding and strain hardening phenomena. **Figure 7b** presents the U_{diss} of this DN gel as a function of the maximum imposed strain, ε_{max}, obtained from the uniaxial cyclic tensile test (**Figure S3**). The dissipation, U_{diss}, increases with ε_{max} above a threshold strain of $\varepsilon_{max} \approx 0.5$. Below the threshold strain, the amount of internal fracturing is negligibly small because of the extensibility of the first network.[19,25,49]

To obtain the correlation, I–U_{diss}, we first measured the fluorescence intensity, I, of stretched specimens of the DN gel fed with NIPAAm and ANS. We used six individual gel specimens, each of which was stretched to a prescribed strain (ε_{max} = 0.5, 0.6, 0.8, 1.5, 2.1, or 3.3). The result clearly shows that I monotonically increased with ε_{max} above a threshold strain of $\varepsilon_{max} \approx 0.5$ (**Figure 7c**). The threshold strain for I is in good agreement with that of U_{diss} (**Figure 7b**), implying that I directly correlates to U_{diss}. The correlation between I and U_{diss} is then obtained by combining the I–ε_{max} plot (**Figure 7c**) and U_{diss}–ε_{max} plot (**Figure 7b**). Here, each ε_{max} value in the I–ε_{max} plot is converted into the U_{diss} value using a polynomial regression in the

U_{diss}–ε_{max} plot (fitted curve in **Figure 7b**). As shown in **Figure 7d**, I exhibits a nearly linear correlation with U_{diss} and the linear regression goes through the origin (I, U_{diss}) = (0, 0), indicating that the fluorescence intensity I reflects the degree of damage quantitatively. The relation between I and U_{diss} or I and ε_{max} obtained from the tensile test should be applicable as calibration curves to estimate the dissipation and the strain field around the crack tip from the fluorescence intensity. It should be mentioned that I does not have to be a linear function of U_{diss} or ε_{max}.

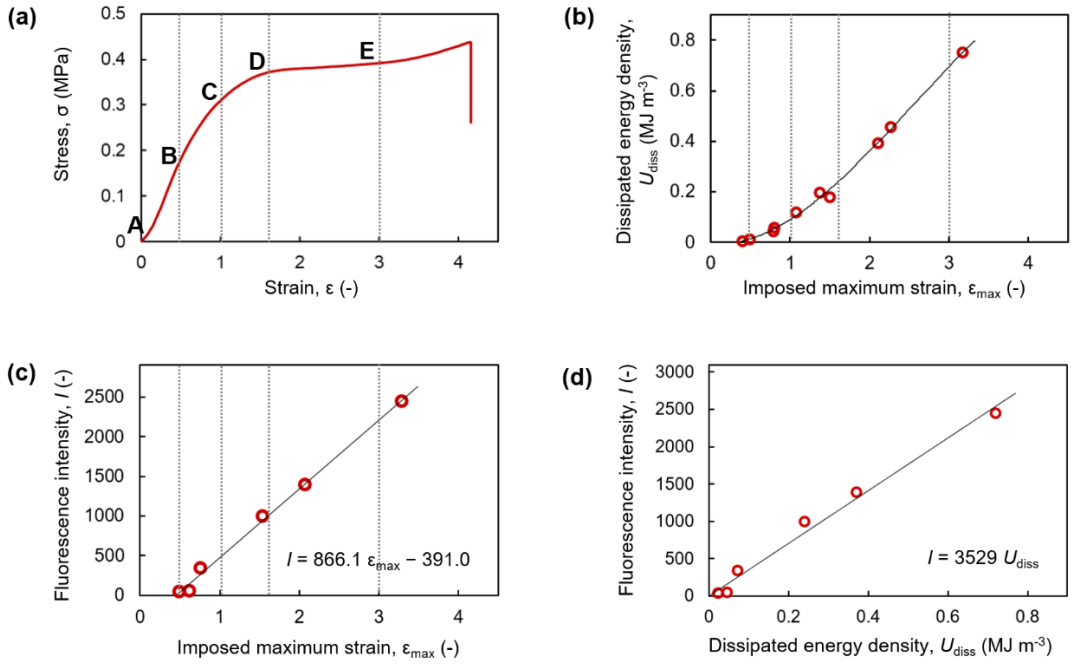

Figure 7. Uniaxial tensile test of a DN gel. **(a)** A uniaxial tensile stress–strain curve, **(b)** dissipated energy density U_{diss} as a function of ε_{max} obtained from the cyclic tensile test (see **Figure S3**), **(c)** fluorescence intensity I as a function of imposed maximum strain ε_{max} after the uniaxial stretching, and **(d)** I as a function of U_{diss} obtained from (b) and (c). The solid lines in (b)–(d) are approximated fitting curves. A polynomial fit ($U_{diss} = -0.0190\ \varepsilon_{max}^3 + 0.1456\ \varepsilon_{max}^2 - 0.0335\ \varepsilon_{max} - 0.0028$) in (b) and linear fits in (c) and (d) are applied.

Since the fluorescence intensity I has good correlations with ε_{max} and U_{diss}, we can obtain the ε_{max} and U_{diss} distributions experienced in the damage zone near a fractured surface from the recorded fluorescence intensity profile. In this characterization, we assumed that the deformation around a crack tip is approximated as uniaxial tension. Although the deformation near the crack tip should be more complicated, uniaxial approximation is usually used to characterize the crack tip field of soft materials[42,50] and a theoretical analysis has suggested that uniaxial tension dominates at least ahead of the crack tip of a highly deformable soft solid under mode-I plane-stress condition.[51,52] With this uniaxial assumption, we can convert the distribution of fluorescence intensity $I(z)$ into $\varepsilon_{max}(z)$ and $U_{diss}(z)$ using the results of uniaxially stretched samples. Linear regressions (**Figures 7c and 7d**) are used as calibration curves. **Figure 8a** shows the fluorescence intensity profile, $I(z)$, of a torn surface of this DN gel along the z direction (see **Figure 4** for the coordinate axis). The linear scales of ε_{max} and U_{diss} converted from I are also shown. Note that an ε_{max} value that is less than 0.5 is not reliable because it is below the threshold of exhibiting fluorescence. The inset letters A, B, C**,** and D in **Figure 8a** correspond to those shown in **Figure 7a**. The observed maximum fluorescence intensity near the torn surface almost corresponded to the fluorescence intensity at yielding point under uniaxial stretching. The damage zone predominantly corresponds to the pre-yielding region with small strain ($0.5 < \varepsilon < 1.6$ for this gel). Because there should be the yielded region closer to the crack tip, this result implies that the size of the yielded region is close to or less than the spatial resolution of current experiment (~50 μm) and is much narrower than the pre-yielding region (~1000–1500 μm).

We can also obtain the maximum stress profile $\sigma_{max}(z)$ imposed around the crack tip from the $\varepsilon_{max}(z)$ profile (**Figure 8a**) and the stress–strain curve (**Figure 7a**) (see **Figure S4** for the detailed procedure). **Figure 8b** shows the $\sigma_{max}(z)$ profile thus obtained. Note that a σ_{max} value that is below 0.17 MPa cannot be obtained because of the fluorescence threshold (see B in **Figure 7a**). The results show that stress increases rapidly with decreasing z (i.e., approaching the fractured surface) and at $z < 400$ μm, the stress increase slows down, exhibiting a saturation tendency, which is more clearly observed in the inset double-logarithm plot. This result implies that, while an asymptotic-like stress field formed at $z > 400$ μm, the stress concentration near the crack tip was moderated perhaps due to internal fracturing or the non-linear mechanical property.

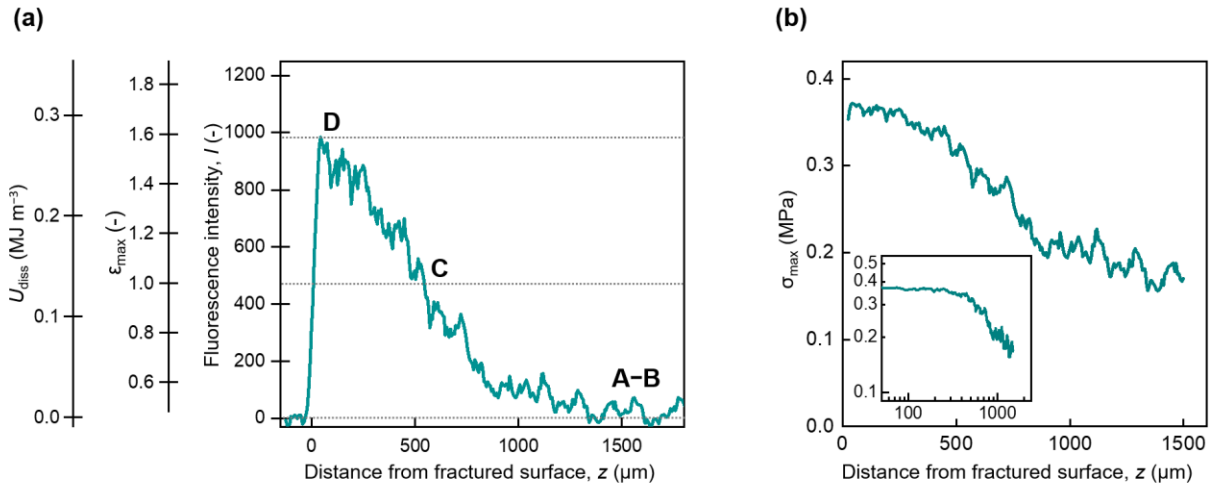

Figure 8. (a) Fluorescence intensity profile $I(z)$ along with the scales of imposed maximum strain ε_{max} and dissipated energy density U_{diss}. **(b)** Imposed maximum stress profile σ_{max} near the fractured surface. The inset is the double-logarithm plot. The scales ε_{max} and U_{diss} in (a) and profile $\sigma_{max}(z)$ in (b) are estimated from the fluorescence data in **Figure 8a** using the tensile results in **Figure 7** as calibration curves.

Advantages and limitations of this technique

Finally, we discuss the advantages and limitations of our method of characterizing the damage zone, in comparison with the other methods. The reported method of characterizing the DN gel is the microscopic observation of the heterogeneity using an optical microscope.[31,32] While the previous method requires re-swelling of the fractured samples to visualize the structural heterogeneity, the current method requires a more complicated procedure using NIPAAm, ANS, and an oxygen-free environment. However, the current method has considerable advantages. First, it can characterize quantitative stress, strain, and energy dissipation profiles, as shown in **Figure 8**, while the previous method cannot. Second, the current method performs observations on as-fractured samples, which results in high spatial accuracy, while the previous method required the re-swelling of the samples, resulting in the overestimation of the damage-zone size. The third advantage is that, using the confocal microscopy technique, the current fluorescence method can observe the three-dimensional distribution of the internal fracturing (**Figure 3c**), while the previous method only provides information on two-dimensional distribution.

Recently, mechanophores have been applied to characterize the fracture of polymeric materials, including single network hydrogels and multiple-network elastomers.[17,40,42] This technique is potentially applicable in the visualization and quantification of the damage distribution of DN gels. However, this technique requires the chemical incorporation of the specific mechanophore into the polymer network, which may affect the network structure and properties.[17,37] Synthesizing a hydrogel with a mechanophore is challenging because most of the reported mechanophores are hydrophobic. Even if the desired network structure is synthesized, the rupture force of the network decreases because of the use of the mechanophore with a weaker scissile bond that needs to be ruptured before the other covalent bonds in the network. In

addition, mechanophores are hardly available in the market at present, which hinders facile use or large-lot experiments. Our mechanoradical polymerization technique is almost free from these limitations. Because no mechanophore incorporation is required, our method can easily characterize various DN hydrogels with the homolytic covalent bond rupture. Chemicals NIPAAm monomer and ANS fluorophore are readily available. Our technique is currently limited because the method based on NIPAAm and ANS is only applicable to hydrogels. To apply this technique to organogels or solvent-free elastomers, a suitable combination of monomer and fluorophore is required. The intrinsic resolution of our technique is the size of tethered PNIPAAm (~10s–100s nm) as discussed above, while that of the mechanophore technique is the size of the mechanophore molecule or the broken polymer strand (~1–10s nm). However, the practical resolution should be limited by the optical system, such as a microscope or a video camera, which is usually larger than these intrinsic resolutions.

Finally, our approach is not based on real-time observation but on posterior observation. Although our method cannot monitor the real-time bond scission around the opening crack in-situ, the posterior observation is complementary to the real-time one. An advantage of the posterior observation is its applicability in the characterization of the complicated deformation or high-speed fracture by recording the fracture history. For example, our technique can be applied in the characterization of the needle-puncture and dynamic fracture whereby the crack propagation is as fast as the shear wave speed of ~10 m s^{-1},[53] whose detection using real-time techniques is difficult. Some mechanophores such as dioxetane[17,36,54] are applicable in real-time observation, while other mechanophores such as π-extended anthracene adduct[40,55] and anthracene dimer[56] enable posterior observation.

CONCLUSION

We developed a new method of visualizing the submillimeter to millimeter-scale damage zone of DN gels around the crack tip by combining the mechanoradical polymerization of NIPAAm, environment-responsive fluorescent probe ANS, and laser scanning confocal microscopy. The damage zone recorded by PNIPAAm is clearly observed as a two- or three-dimensional fluorescence image. The damage distribution was quantitatively captured as a fluorescence intensity map or line profile. By calibrating the fluorescence intensity using tensile data, the profiles of the maximum strain and stress imposed, and the dissipated mechanical energy density in the damage zone of a DN gel are quantitatively estimated.

Our method bears three key advantages: (1) it allows for the quantitative characterization of the damage distribution in two and three dimensions with high spatial accuracy, (2) it does not require the incorporation of specific mechanophores into the polymer network, and (3) it allows for the characterization of high-speed fractures or complicated deformations by recording the damage history. Owing to these prominent advantages, we believe that this method will be used to characterize the crack tip field of various DN gels, which will advance the fracture mechanics of tough soft materials. Additionally, this mechanoradical polymerization technique is also potentially applicable in the detection and characterization of the polymer chain scission of other hydrogels, as demonstrated by the observation of the fractured surface of a single-network hydrogel.

ASSOCIATED CONTENT

Supporting Information

The following files are available:

Supporting Methods and Figures S1–S4 (PDF).

AUTHOR INFORMATION

Corresponding Authors

*E-mail: tkhr.matsuda@gmail.com (T.M.); gong@sci.hokudai.ac.jp (J.P.G.).

Author Contributions

#Takahiro Matsuda and Runa Kawakami contributed to this study equally. The manuscript was written through contributions of all authors.

Note

The authors declare no competing financial interests.

Note for review only

The first draft has been deposited on ChemRxiv.

ACKNOWLEDGMENT

This research was partially funded by a Grant-in-Aid for JSPS Research Fellow (No. 17J09290) and for Scientific Research (S) (No. 17H06144) from the Japan Society for the Promotion of

Science, and by the ImPACT Program of the Council for Science, Technology and Innovation (Cabinet Office, Government of Japan). The authors thank Toagosei Co., Ltd. for providing AMPS and NaAMPS. Takahiro Matsuda and Runa Kawakami are grateful to the Nikon Imaging Center at Hokkaido University and Kentaro Kobayashi for their help with confocal microscopy, image acquisition, and analysis.

REFERENCES

(1) Creton, C. 50th anniversary perspective: Networks and gels: Soft but dynamic and tough. *Macromolecules* **2014**, *47* (19), 6783−6790.

(2) Long, R.; Hui, C.-Y. Fracture toughness of hydrogels: Measurement and interpretation. *Soft Matter* **2016**, *12* (39), 8069−8086.

(3) Fan, H.; Gong, J. P. Fabrication of bioinspired hydrogels: Challenges and opportunities. *Macromolecules* **2020,** *53* (8), 2769–2782.

(4) Bai, R.; Yang, J.; Suo, Z. Fatigue of hydrogels. *Eur. J. Mech. A Solids* **2019**, *74*, 337−370.

(5) Grijalvo, S.; Eritja, S.; Díaz, D. D. On the race for more stretchable and tough hydrogels. *Gels* **2019**, *5*, 24.

(6) Fuchs, S.; Shariati, K.; Ma, M. Specialty tough hydrogels and their biomedical applications. *Adv. Healthcare Mater.* **2020**, *9*, 1901396.

(7) Annabi, N.; Tamayol, A.; Uquillas, J. A.; Akbari, M.; Bertassoni, L. E. Cha, C.; Camci-Unal, G.; Dokmeci, M. R. Peppas, N. A.; Khademhosseini, A. 25th anniversary article: Rational

design and applications of hydrogels in regenerative medicine. *Adv. Mater.* **2014**, *26*, 85–124.

(8) Rus, D.; Tolley, M. Design, fabrication and control of soft robots. *Nature* **2015**, *521*, 467–475.

(9) Polygerinos, P.; Correll, N.; Morin, A. A.; Mosadegh, B.; Onal, C. D.; Petersen, K.; Cianchetti, M.; Tolley, M. T.; Shepherd, R. F. Soft robotics: Review of fluid-driven intrinsically soft devices; manufacturing, sensing, control, and applications in human-robot interaction. *Adv. Eng. Mater.* **2017,** *19*, 1700016.

(10) Rogers, J. A.; Someya, T.; Huang, Y. Materials and mechanics for stretchable electronics. *Science* **2010**, *327*, 1603–1607.

(11) Lim, H.-R.; Kim, H. S.; Qazi, R.; Kwon, Y. T.; Jeong, J.-W. Yeo, W.-H. Advanced soft materials, sensor integrations, and applications of wearable flexible hybrid electronics in healthcare, energy, and environment. *Adv. Mater.* **2020**, *32*, 1901924.

(12) Gong, J. P.; Katsuyama, Y.; Kurokawa, T.; Osada, Y. Double-network hydrogels with extremely high mechanical strength. *Adv. Mater.* **2003**, *15*, 1155−1158.

(13) Gong, J. P. Why are double network hydrogels so tough? *Soft Matter* **2010**, *6*, 2583−2590.

(14) Chen, Q.; Chen, H.; Zhu, L.; Zheng, J. Fundamentals of double network hydrogels. *J. Mater. Chem. B* **2015**, *3*, 3654−3676.

(15) Nakajima, T. Generalization of the sacrificial bond principle for gel and elastomer toughening. *Polym. J.* **2017**, *49*, (6), 477−485.

(16) Sun, J.-Y.; Zhao, X.; Illeperuma, W. R. K.; Chaudhuri, O.; Oh, K. H.; Mooney, D. J.; Vlassak, J. J.; Suo, Z. Highly stretchable and tough hydrogels. *Nature* **2012**, *489*, 133−136.

(17) Ducrot, E.; Chen, Y.; Bulters, M.; Sijbesma, R. P.; Creton, C. Toughening elastomers with sacrificial bonds and watching them break. *Science* **2014**, *344*, 186−189.

(18) Matsuda, T.; Nakajima, T.; Gong, J. P. Fabrication of tough and stretchable hybrid double-network elastomers using ionic dissociation of polyelectrolyte in nonaqueous media. *Chem. Mater.* **2019**, *31*, 3766−3776.

(19) Ahmed, S.; Nakajima, T.; Kurokawa, T.; Anamul Haque, M.; Gong, J. P. Brittle−ductile transition of double network hydrogels: Mechanical balance of two networks as the key factor. *Polymer* **2014**, *55* (3), 914−923.

(20) Tanaka, Y.; Kuwabara, R.; Na, Y.-H.; Kurokawa, T.; Gong, J. P.; Osada, Y. Determination of fracture energy of high strength double network hydrogels. *J. Phys. Chem. B* **2005,** *109*, 11559–11562.

(21) Nakajima, T.; Kurokawa, T.; Furukawa, H.; Gong, J. P. Effect of constituent networks of double-network gels on their mechanical properties and energy dissipation process. *Soft Matter* **2020,** Published Online (https://doi.org/10.1039/D0SM01057J).

(22) Zhang, W.; Liu, X.; Wang, J.; Tang, J.; Hu, J.; Lu, T.; Suo, Z. Fatigue of double-network hydrogels. *Eng. Fract. Mech.* **2018**, *187*, 74−93.

(23) Na, Y.-H.; Tanaka, Y.; Kawauchi, Y.; Furukawa, H.; Sumiyoshi, T.; Gong, J. P.; Osada, Y. Necking phenomenon of double-network gels. *Macromolecules* **2006**, *39*, 4641−4645.

(24) Webber, R. E.; Creton, C.; Brown, H. R.; Gong, J. P. Large strain hysteresis and Mullins effect of tough double-network hydrogels. *Macromolecules* **2007**, *40*, 2919−2927.

(25) Nakajima, T.; Kurokawa, T.; Ahmed, S.; Wu, W.-L.; Gong, J. P. Characterization of internal fracture process of double network hydrogels under uniaxial elongation. *Soft Matter* **2013**, *9*, 1955−1966.

(26) Matsuda, T.; Nakajima, T.; Fukuda, Y.; Hong, W.; Sakai, T.; Kurokawa, T.; Chung, U.-I.; Gong, J. P. Yielding criteria of double network hydrogels. *Macromolecules* **2016**, *49* (5), 1865−1872.

(27) Matsuda, T.; Kawakami, R.; Namba, R.; Nakajima, T.; Gong, J. P. Mechanoresponsive self-growing hydrogels inspired by muscle training. *Science* **2019**, *363*, 504−508.

(28) Brown, H. R. A model of the fracture of double network gels. *Macromolecules* **2007**, *40* (10), 3815−3818.

(29) Tanaka, Y. A local damage model for anomalous high toughness of double-network gels. *Europhys. Lett.* **2007**, *78* (5), 56005.

(30) Tanaka, Y.; Kawauchi, Y.; Kurokawa, T.; Furukawa, H.; Okajima, T.; Gong, J. P. Localized yielding around crack tips of double-network gels. *Macromol. Rapid Commun.* **2008**, *29* (18), 1514−1520.

(31) Yu, Q. M.; Tanaka, Y.; Furukawa, H.; Kurokawa, T.; Gong, J. P. Direct observation of damage zone around crack tips in double-network gels. *Macromolecules* **2009**, *42* (12), 3852−3855.

(32) Liang, S.; Wu, Z. L.; Hu, J.; Kurokawa, T.; Yu, Q. M.; Gong, J. P. Direct observation on the surface fracture of ultrathin film double-network hydrogels. *Macromolecules* **2011**, *44*, 3016–3020.

(33) Stratigaki, M.; Göstl, R. Methods for exerting and sensing force in polymer materials using mechanophores. *ChemPlusChem* **2020**, *85*, 1–10.

(34) Celestine, A.-D. N.; Beiermann, B. A.; May, P. A.; Moore, J. S.; Sottos, N. R.; White, S. R. Fracture-induced activation in mechanophore-linked, rubber toughened PMMA. *Polymer* **2014**, *55*, 4164–4171.

(35) Wang, Q.; Gossweiler, G. R.; Craig, S. L.; Zhao, X. Mechanics of mechanochemically responsive elastomers. *J. Mech. Phys. Solids* **2015**, *82*, 320–344.

(36) Clough, J. M.; Creton, C.; Craig, S. L.; Sijbesma, R. P. Covalent bond scission in the mullins effect of a filled elastomer: Real-time visualization with mechanoluminescence. *Adv. Funct. Mater.* **2016**, *26*, 9063–9074.

(37) Millereau, P.; Ducrot, E.; Clough, J. M.; Wiseman, M. E.; Brown, H. R.; Sijbesma, R. P.; Creton, C. Mechanics of elastomeric molecular composites. *Proc. Natl. Acad. Sci. U.S.A.* **2018**, *115* (37) 9110−9115.

(38) Celestine, A.-D. N.; Sottos, N. R.; White, S. R. Strain and stress mapping by mechanochemical activation of spiropyran in poly(methyl methacrylate). *Strain* **2019**, *55*, e12310.

(39) Kim, T. A.; Lamuta, C.; Kim, H.; Leal, C.; Sottos, N. R. Interfacial force-focusing effect in mechanophore-linked nanocomposites. *Adv. Sci.* **2020**, 1903464.

(40) Stratigaki, M.; Baumann, C.; van Breemen, L. C. A.; Heuts, J. P. A.; Sijbesma, R. P.; Göstl, R. Fractography of poly(*N*-isopropylacrylamide) hydrogel networks crosslinked with mechanofluorophores using confocal laser scanning microscopy. *Polym. Chem.* **2020**, *11*, 358−366.

(41) Lin, Y.; Barbee, M. H.; Chang, C.-C.; Craig, S. L. Regiochemical effects on mechanophore activation in bulk materials. *J. Am. Chem. Soc.* **2018,** *140*, 15969–15975.

(42) Chen, Y.; Yeh, C. J.; Qi, Y.; Long, R.; Creton, C. From force-responsive molecules to quantifying and mapping stresses in soft materials. *Sci. Adv.* **2020,** *6*, eaaz5093.

(43) Wang, L.-J.; Yang, K.-X.; Zhou, Q.; Yang, H.-Y.; He, J.-Q.; Zhang, X.-Y. Rhodamine mechanophore functionalized mechanochromic double network hydrogels with high sensitivity to stress. *Chinese J. Polym. Sci.* **2020,** *38*, 24–36.

(44) Schild, H. G. Poly(*N*-isopropylacrylamide): Experiment, theory and application. *Prog. Polym. Sci.* **1992**, *17*, 163−249.

(45) Turner, D. C.; Brand, L. Quantitative estimation of protein binding site polarity. Fluorescence of *N*-arylaminonaphthalenesulfonates. *Biochemistry* **1968**, *7*, 3381–3390.

(46) Ito, D.; Itagaki, H. Clarification of the inner microenvironments in poly(*N*-isopropylacrylamide) hydrogels in macrogel and microgel forms using a fluorescent probe technique. *Eur. Polym. J.* **2018**, *99*, 277–283.

(47) Lake, G. J.; Thomas, A. G. The strength of highly elastic materials. *Proc. R. Soc. London, Ser. A* **1967**, A300, 108–119.

(48) Akagi, Y.; Sakurai, H.; Gong, J. P.; Chung, U.-I.; Sakai, T. Fracture energy of polymer gels with controlled network structures. *J. Chem. Phys.* **2013**, *139* (14), 144905.

(49) Mai, T.-T.; Matsuda, T.; Nakajima, T.; Gong, J. P.; Urayama, K. Distinctive characteristics of internal fracture in tough double network hydrogels revealed by various modes of stretching. *Macromolecules* **2018**, *51*(14), 5245–5257.

(50) Mzabi, S.; Berghezan, D.; Roux, S.; Hild, F.; Creton, C. A critical local energy release rate criterion for fatigue fracture of elastomers. *J. Polym. Sci. B: Polym. Phys.* **2011,** *49*, 1518–1524.

(51) Long, R.; Hui, C. Y. Crack tip fields in soft elastic solids subjected to large quasi-static deformation — A review. *Extreme Mech. Lett.* **2015**, *4*, 131–155.

(52) Long, R.; Hui, C.-Y.; Gong, J. P.; Bouchbinder, E. The fracture of highly deformable soft materials: A tale of two length scales. *Annual Rev. Cond. Matter Phys.* **2020**, *12*, in press. Preprint: [arXiv:2004.03159]

(53) Kolvin, I.; Kolinski, J. M.; Gong, J. P.; Fineberg, J. How supertough gels break. *Phys. Rev. Lett.* **2018,** *121*, 135501.

(54) Chen, Y.; Spiering, A. J. H.; Karthikeyan, S.; Peters, G. W. M.; Meijer, E. W.; Sijbesma, R. P. Mechanically induced chemiluminescence from polymers incorporating a 1,2-dioxetane unit in the main chain. *Nature Chem.* **2012,** *4*, 559–562.

(55) Göstl, R.; Sijbesma, R. P. π-extended anthracenes as sensitive probes for mechanical stress. *Chem. Sci.* **2016,** *7*, 370–375.

(56) Zhang, H.; Zeng, D.; Pan, Y.; Chen, Y.; Ruan, Y.; Xu, Y.; Boulatov, R.; Creton, C.; Weng, W. Mechanochromism and optical remodeling of multi-network elastomers containing anthracene dimers. *Chem. Sci.* **2019,** *10*, 8367–8373.